Incorportating Spatio-Temporal Convection Effects in Classical Snowball Earth Models

Elizabeth Rose

Supervised by Dr. Robert Marangell
The University of Sydney

February 28, 2021

Abstract

Energy balance models are used to study a system that is dependent on the incoming and outgoing energy, such as the Earth's climate. Budyko (1969) and Sellers (1969) independently suggested similar models of this type to understand long-term global climates. North (1975) extended on these models to incorporate diffusive heat transport. Their models depend on the global albedo, and thus the location of the ice line. This allows for the stability analysis of various ice line locations, including a snowball climate and an ice free climate. By using previously developed albedo functions to model past and present climate, we find both large and small stable ice caps. The stability of the snowball and ice-free states vary with the model considered. We also discuss the effect of rising carbon dioxide levels in the atmosphere on the models, and the effect this has on the location of the ice line.

1 Introduction

Geological evidence suggests that the earth has gone through periods in which much of its surface was covered in glaciers (Hoffman et al. 2020). Two major events of this type, known as snowball earth events, book-ended the Cryogenian period (715 - 635 million years ago (Ma)). The first, known as the Sturtian glaciation, lasted from 715-660 Ma, while the second, the Marinoan glaciation, lasted from 650-635 Ma. Geological evidence shows that following a snowball earth event, atmospheric oxygen levels rose and new life forms evolved.

Energy balance models are useful in studying systems that are dependent on the absorbed energy, for example the long-term climate on Earth. In this report, we describe such a model and discuss the results. We expand on the elementary model proposed by Budyko (1969) and Sellers (1969), by incorporating a diffusion term first proposed by North (1975), as well as accounting for a dynamic ice line through the coupled model proposed by Widiasih (2013). In doing so, the equilibrium states are analysed. The albedo of a surface describes how much light said surface reflects. By using previously proposed alterations to the albedo function, we attempt to model the great glacial episodes of the past.

1.1 Statement of Authorship

In Sections 2, 3 and 5, the author followed the analysis in Walsh (2017). All figures were produced by the author using Python 3.0. Sections 4, 5.2, 6 and 7 are the author's own work, with substantial guidance from their supervisor Dr. Robert Marangell.

2 The Budyko-Sellers Model

Budyko (1969) and Sellers (1969) independently proposed mathematical models to roughly describe the incoming and outgoing energy of the Earth in relation to the surface albedo. While the Sellers model is qualitatively equivalent, in this report we will consider the Budyko model as the basis for our investigation.

The model is an Energy Balance Model (EBM), in which we consider the net change in energy as a function of position. Here, the position on the Earth's surface is denoted by $y = \sin\theta$, where θ denotes the latitude at that point. We assume homogeneity across longitudes, so the model is spatially one-dimensional. We also assume symmetry across the equator, so we take $y \in [0,1]$. The dependant variable in the model is the temperature as a function of position and time, denoted $T(y,t)$.

To form an EBM for the Earth-atmosphere system, we must first consider the distribution of incoming radiation across latitudes. The solar constant measures the amount of radiation from the Sun reaching the surface of the Earth, in units of Watts/m^2. Here, due to the geometry, we consider the parameter Q, which is equal to the solar constant divided by 4 (currently, $Q = 343$ Watts/m^2). We must also consider the fact that more radiation reaches the equator than the poles, and so we scale Q by the function $s(y)$, whose explicit formulation is

$$s(y) = \frac{2}{\pi^2} \int_0^{2\pi} \sqrt{1 - \left(\sqrt{1-y^2}\sin\beta\cos\gamma - y\cos\beta\right)^2}\, d\gamma, \tag{1}$$

where β denotes the obliquity of the Earth's spin axis (McGehee and Lehman 2017) (currently, $\beta = 23.5°$). The other factor that influences the amount of incoming radiation is the albedo - the percentage of radiation that is reflected from a surface. As white ice reflects much more radiation than darker open water, one simple model for the albedo (Budyko 1969) considers one value for ice caps and another for open water. The border between the two regions is called the ice line, and denoted by η. With $\alpha_1 < \alpha_2$, we write the albedo function as

$$\alpha(y,\eta) = \begin{cases} \alpha_1, & y < \eta \\ \alpha_2, & y > \eta \\ (\alpha_1 + \alpha_2)/2 & y = \eta \end{cases} \tag{2}$$

Then, the incoming radiation term is

$$E_{in}(y,\eta) = Qs(y)(1 - \alpha(y,\eta)) \tag{3}$$

The outgoing radiation term can be approximated by the linear term $E_{out} = A + BT$, where A and B are constants determined from satellite data. Currently, $A = 202$ Watts/m^2 and $B = 1.9$ Watts/(m^2 C°).

The final term to consider for the EBM is the transport of heat across latitudes. Budyko and Sellers both considered the linear term $E_{trans} = C(T - \overline{T})$, where C is some constant and $\overline{T}$ is the global annual average temperature, given by

$$\overline{T}(t) = \int_0^1 T(y,t)dy. \tag{4}$$

Then, with R as the heat capacity of Earth's surface, the model is given by

$$R\frac{dT}{dt} = E_{in} - E_{out} + E_{trans} \tag{5}$$

$$= Qs(y)(1 - \alpha(y,\eta)) - (A + BT) - C(T - \overline{T}). \tag{6}$$

2.1 Incorporating Diffusion

An alternate energy transport term was proposed by North (1975), in which the transport is given by a diffusion term, $E_{trans} = D\nabla^2 T(y,t)$ where D is some diffusion coefficient to be determined (see Section 4). ∇^2 indicates the Laplace operator, where $\nabla^2 f = \nabla \cdot (\nabla f)$ and ∇ is the differential operator in Cartesian coordinates. However, this makes the equation no longer an ordinary differential equation, but rather a partial differential equation, and hence increases the complexity of the analysis.

In spherical coordinates with no radial or longitudinal dependence,

$$E_{tran} = D\nabla^2 T = D\frac{\partial}{\partial y}(1-y^2)\frac{\partial T}{\partial y} \tag{7}$$

The system is then

$$R\frac{\partial T}{\partial t} = Qs(y)(1-\alpha(y,\eta)) - (A+BT) + D\frac{\partial}{\partial y}(1-y^2)\frac{\partial T}{\partial y} \tag{8}$$

2.2 A Dynamic Ice Line

The above equations consider a fixed ice line η, however evidence shows that the ice line can move (ice caps grow and shrink) with time. Widiasih (2013) introduced a second, coupled equation into the model that describes the change in η with time. By considering the temperature at the ice line in relation to some critical temperature T_c at which ice melts or forms, η can be said to decrease if $T(\eta,t) > T_c$, and conversely η will increase if $T(\eta,t) < T_c$. This can be expressed as

$$\frac{d\eta}{dt} = \epsilon(T(\eta,t) - T_c), \tag{9}$$

where ϵ is a parameter of order 10^{-13} (McGehee and Widiasih 2014), which describes the slow movement of the ice line in response to changes in temperature.

Incorporating everything above, this report will analyse the coupled PDE model given by

$$R\frac{\partial T}{\partial t} = Qs(y)(1-\alpha(y,\eta)) - (A+BT) + D\frac{\partial}{\partial y}(1-y^2)\frac{\partial T}{\partial y} \tag{10a}$$

$$\frac{d\eta}{dt} = \epsilon\left(T(\eta,t) - T_c\right) \tag{10b}$$

The boundary conditions of the system are that the gradient of the temperature equals zero at the North Pole ($y = 1$) and equator ($y = 0$). This is equivalent to ensuring there is no heat transport across the poles or equator.

3 Analysis by the Spectral Method

To approximate solutions to the model, we follow the analysis of Walsh (2017). Due to the assumed symmetry across the equator, the functions of y in system (10) are even. As the Legendre polynomials are eigenfunctions

of the spherical Laplace operator, it is thus logical to approximate the system by expanding each function of y in terms of the first $N + 1$ even Legendre polynomials $p_{2n}(y)$. Furthermore, the properties of the Legendre polynomials at $y = 0, 1$ ensure that the solution matches the boundary conditions.

We write

$$T(y, t) = \sum_{n=0}^{N} T_{2n}(t) p_{2n}(y). \tag{11}$$

By the properties of Legendre polynomials, expression (11) fits the prescribed boundary conditions, noting that

$$\nabla T = T_{2n}(t) \sqrt{1 - y^2} \frac{dp_{2n}}{dy} \tag{12}$$

for our case.

We also want to expand $s(y)$ and $s(y)\alpha(y, \eta)$ in terms of Legendre polynomials. The explicit formulation of $s(y)$ is given above in (1). Writing

$$s(y) = \sum_{n=0}^{\infty} s_{2n} p_{2n}(y) \tag{13}$$

where s_{2n} is given by

$$s_{2n} = (4n + 1) \int_0^1 s(y) p_{2n}(y) dy, \tag{14}$$

we find that for $n > 1$, s_{2n} is small, and thus the function can be approximated uniformly to within 3% by

$$s(y) = s_0 p_0(y) + s_2 p_2(y) \tag{15}$$

with $s_0 = 1$, $s_2 = -0.477$, $p_0(y) = 1$ and $p_2(y) = \frac{1}{2}(3y^2 - 1)$ (Walsh 2017).

To expand $s(y)\alpha(y, \eta)$ in terms of the first $N + 1$ even Legendre polynomial, we write

$$s(y)\alpha(y, \eta) = \sum_{n=0}^{N} \overline{\alpha}_{2n} p_{2n}(y) \tag{16}$$

where

$$\begin{aligned}
\bar{\alpha}_{2n}(\eta) &= (4n + 1) \int_0^1 \alpha(y, \eta) s(y) p_{2n}(y) dy \\
&= (4n + 1) \left(\alpha_1 \int_0^\eta s(y) p_{2n}(y) dy + \alpha_2 \int_\eta^1 s(y) p_{2n}(y) dy \right) \\
&= (4n + 1) \left(\alpha_2 \int_0^1 s(y) p_{2n}(y) dy - (\alpha_2 - \alpha_1) \int_0^\eta s(y) p_{2n}(y) dy \right) \\
&= \alpha_2 s_{2n} - (4n + 1)(\alpha_2 - \alpha_1) \int_0^\eta s(y) p_{2n}(y) dy.
\end{aligned} \tag{17}$$

Then, noting that

$$\begin{aligned}
\frac{d}{dy}(1 - y^2) \frac{dp_{2n}}{dy} &= (1 - y^2) \frac{2n}{(y^2 - 1)^2} (2y p_{2n-1}(y) + ((2n - 1)y^2 - 2n - 1) p_{2n}(y) \\
&\qquad\qquad\qquad\qquad\qquad - 2y \frac{2n}{y^2 - 1} (y p_{2n}(y) - p_{2n-1}(y)) \\
&= \frac{2n}{y^2 - 1} (-2y^2 - ((2n - 1)y^2 - 2n - 1) p_2 n(y) \\
&= -2n(2n + 1) p_{2n}(y)
\end{aligned}$$

4

(10a) becomes

$$R \sum_{n=0}^{N} \dot{T}_{2n} p_{2n}(y) = Q \sum_{n=0}^{N} (s_{2n} - \bar{\alpha}_{2n}) p_{2n}(y) - A - B \sum_{n=0}^{N} T_{2n} p_{2n}(y) - D \sum_{n=0}^{N} 2n(2n+1) T_{2n} p_{2n}(y) \quad (18)$$

Equating coefficients of p_{2n}, system (10) becomes (Walsh 2017)

$$R\dot{T}_0 = Q(s_0 - \bar{\alpha}_0(\eta)) - A - BT_0 \quad (19a)$$

$$R\dot{T}_{2n} = Q(s_{2n} - \bar{\alpha}_{2n}(\eta)) - (B + 2n(2n+1)D)T_{2n}, n = 1, \ldots, N \quad (19b)$$

$$\dot{\eta} = \epsilon \left(\sum_{n=0}^{N} T_{2n} p_{2n}(\eta) - T_c \right) \quad (19c)$$

3.1 Fenichel's Theorem

Consider a system of the form

$$\dot{x} = f(x, u, \epsilon) \quad (20a)$$

$$\dot{u} = \epsilon g(x, u, \epsilon) \quad (20b)$$

where $x \in \mathbb{R}^n, u \in \mathbb{R}^m$ and $\epsilon \in \mathbb{R}$ a parameter. Assume f, g are C^∞ on $\mathbb{R}^{n+m} \times I$, where I is an open interval containing 0. Define the set of rest points when $\epsilon = 0$ as

$$\Lambda^0 = \{(x, u) : f(x, u, 0) = 0\} = \{(x, u) : x = h^0(u)\} \quad (21)$$

Note that λ^0 is the graph of a C^∞ function $h^0(u)$. Assume that Λ^0 is normally hyperbolic with respect to system (20) when $\epsilon = 0$ (Walsh 2017).

Theorem 3.1. *If ϵ is positive and sufficiently small, there exists a manifold Λ^ϵ within $O(\epsilon)$ of Λ^0 and diffeomorphic to Λ^0. In addition, Λ^ϵ is locally invariant under the flow of (20) and C^r for any $r < \infty$.*

As we assume the ice line moves slowly in response to changes in temperature, it follows that η is a slow variable, while $T_0, \ldots, T_{2n}$ are fast variables. Then, if $\epsilon = 0$, η is fixed and

$$T_0 \to \frac{1}{B}(Q(s_0 - \bar{\alpha}_0(\eta) - A) =: f_0(\eta) \quad (22)$$

$$T_{2n} \to \frac{Q(s_{2n} - \bar{\alpha}_{2n}(\eta))}{B + 2n(2n+1)D} =: f_{2n}(\eta) \quad n = 1, \ldots, N \quad (23)$$

That is, system (19) has a globally attracting curve of rest points, namely $\Lambda^0 = \{(x, \eta) : x = h^0(\eta)\}$, where

$$x = h^0(\eta) = (f_0(\eta), f_2(\eta), \ldots, f_{2N}(\eta)). \quad (24)$$

By Fenichel's Theorem 3.1, it follows that (19) has an attracting invariant manifold for sufficiently small ϵ, on which the dynamics are well approximated by the single ODE (Walsh 2017; Widiasih 2013)

$$\dot{\eta} = \epsilon \left(\sum_{n=0}^{N} f_{2n}(\eta) p_{2n}(\eta) - T_c \right) = \epsilon h(\eta). \quad (25)$$
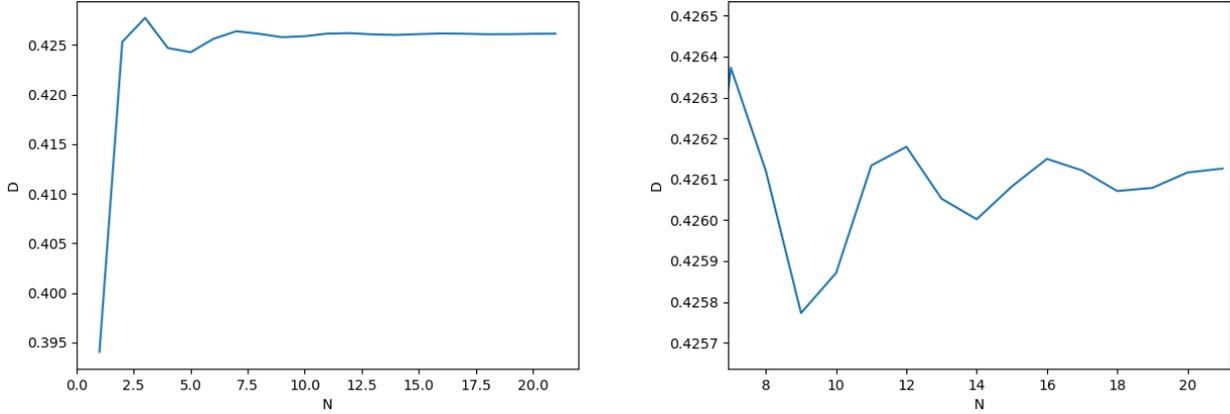
Figure 1: Plot showing how D varies as N increases. Right: zoomed to exclude $N = 1 - 7$. Over the first few values of N, the computed value of D varies significantly, however the value begins to stabilise at about $N = 10$. For $N \geq 15$, $D = 0.4261$ to four decimal places.

4 Calculating the Diffusion Coefficient D

To determine the value of the diffusion coefficient D, we fit the current climate such that our current state corresponds to a point of stable equilibrium. Using the definition of $h(\eta)$ in (25), we require that $h(0.94) = 0$ and $h'(0.94) < 0$ (our current ice line is approximately $\eta = 0.94$, (Walsh 2017)). As we only have one parameter to determine, the first expression is sufficient for the calculation, while the second is used to check stability.

Using Newton's method of approximation, we can write

$$D_{i+1} = D_i - \frac{\sum_{n=0}^{N} f_{2n}(0.94) p_{2n}(0.94) - T_c}{\sum_{n=0}^{N} \left. \frac{df_{2n}}{dD} \right|_{\eta=0.94} p_{2n}(0.94)}, \tag{26}$$

where D_i is a previous approximation for D, and D_{i+1} is the new approximation.

It is clear that the above expression is heavily dependant on N. In an ideal world, we would let $N \to \infty$ as this would depict the analytic solution exactly. However, the computation increases complexity as N increases, and hence computation time increases. Thus, it is desirable to know how large N must be to reach some limit of error. It would be ideal to set this error as the order of ϵ (10^{-13}), however we were unable to reach this due to limitations in computing power, and thus we aim for an error of the order 10^{-4}. Note that here, as we do not know the actual value of D, error refers to the difference between the current computed value and the previous.

For each value of N, an approximation for D accurate to 10^{-13} was calculated using the above expression iteratively. The results of these calculations are plotted in Figure 1. We can see that after $N = 10$, the value of D begins to stabilise, and a closer look at the values shows that we require $N \geq 15$ for an error of 10^{-4}, where $D = 0.4261$.

6
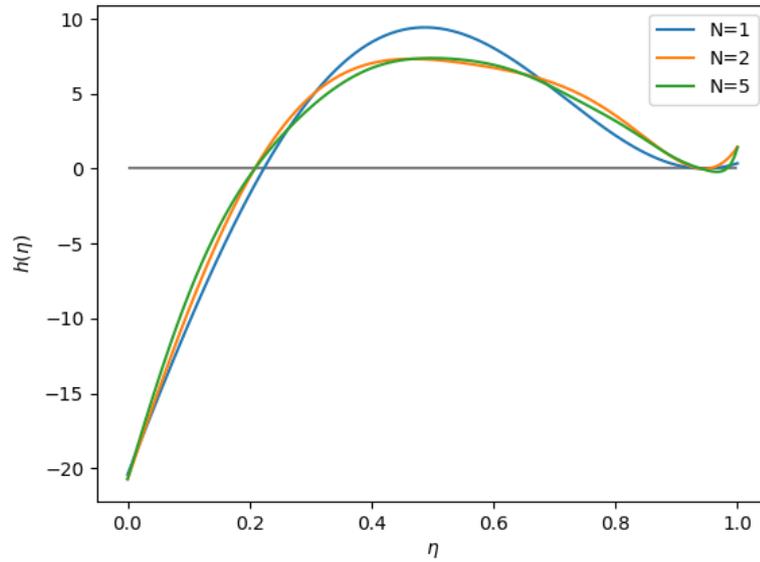
Figure 2: Plot of the dynamics function $h(\eta)$ (25) showing the temperature at the ice line relative to T_c, plotted for $N = 1, 2, 5$. As $h(0) < 0$ and $h(1) > 0$, both the snowball state and ice-free state are stable. By construction (by calculating D), the curves all cross at the stable equilibrium of $\eta = 0.94$. There is also a large unstable ice cap at about $\eta = 0.2$.

4.1 Plotting solutions

Using the above values for D, we can plot the function $h(\eta)$ as defined above in (25). This function shows the temperature at the ice line relative to the the critical temperature T_c. That is, if $h(\eta) > 0$, ice will melt and the ice line will be pushed poleward ($\eta \to 1$), while if $h(\eta) < 0$, ice will form and the ice line will be pushed towards the equator ($\eta \to 0$). If $h(\eta^*) = 0$, then η^* is a equilibrium point, whose stability is determined by the sign of $h'(\eta^*)$.

With the parameters set as

$$Q = 343, A = 202, B = 1.9, \alpha_1 = 0.32, \alpha_2 = 0.62, T_c = -10, \tag{27}$$

(Walsh 2017) and using the corresponding D value for each value of N, we can plot the graph of $h(\eta)$, as shown in Figure 2.

The parameter A can be thought of as a proxy for carbon dioxide levels in the atmosphere, where a low value for A corresponds to higher CO_2 values and a high value of A corresponds to lower CO_2 values. As such, the bifurcation diagram showing the equilibrium values of η as A varies is of interest. This diagram has been plotted in Figure 3.
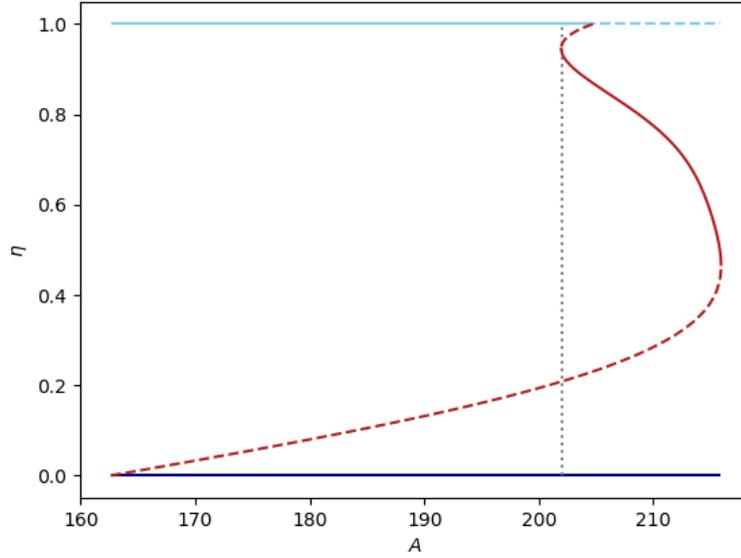
Figure 3: Bifurcation diagram for parameter A, $N = 2, D = 0.4261$. Dashed - unstable equilibria, solid - stable equilibria. Dotted line - our current climate. We can see in this figure that if our CO_2 levels increase (a decrease in A) much beyond our current value, we will move directly towards the ice-free state. This supports evidence of global warming and melting ice caps.

5 The Jormungand Model

To model the great glacial episodes of the Neoproterozoic era, a large stable ice cap must be a solution. This is not seen in the above system, so a new albedo function is considered. We fix a latitude $y = \rho$ and assume any ice forming at latitudes $y < \rho$ are free of snow, leading to a third albedo value α_i, where $\alpha_1 < \alpha_i < \alpha_2$ (Walsh 2017). This gives the function

$$\alpha_J(y, \eta) = \begin{cases} a(y, \eta), & \eta < \rho \\ b(y, \eta), & \eta \geq \rho \end{cases} \tag{28}$$

where

$$a(y, \eta) = \begin{cases} \alpha_1, & y < \eta \\ \alpha_i, & \eta < y < \rho \\ \alpha_2, & y > \rho \end{cases} \quad \text{and} \quad b(y, \eta) = \begin{cases} \alpha_1, & y < \eta \\ \alpha_2, & y > \eta \end{cases}. \tag{29}$$

We again need to expand this function in terms of the first N even Legendre polynomials, so we calculate the coefficients as follows (Walsh 2017). We write

$$s(y)\alpha(y, \eta) = \sum_{n=0}^{N} \overline{\alpha}_{2n, J} p_{2n}(y) = \sum_{n=0}^{N} p_{2n}(y) \begin{cases} \overline{a}_{2n}(\eta), & \eta < \rho \\ \overline{b}_{2n}(\eta), & \eta \geq \rho \end{cases}. \tag{30}$$

Then, $\bar{b}_{2n}(\eta)$ is given by (17) above:

$$
\begin{aligned}
\bar{b}_{2n}(\eta) &= (4n+1) \int_0^1 b(y,\eta) s(y) p_{2n}(y) dy \\
&= \alpha_2 s_{2n} - (4n+1)(\alpha_2 - \alpha_1) \int_0^\eta s(y) p_{2n}(y) dy
\end{aligned}
\tag{31}
$$

Similarly, we compute

$$
\begin{aligned}
\bar{a}_{2n}(\eta) &= (4n+1) \int_0^1 a(y,\eta) s(y) p_{2n}(y) dy \\
&= (4n+1) \left(\alpha_1 \int_0^\eta s(y) p_{2n}(y) dy + \alpha_i \int_\eta^\rho s(y) p_{2n}(y) dy + \alpha_2 \int_\rho^1 s(y) p_{2n}(y) dy \right) \\
&= (4n+1) \left(\alpha_2 \int_0^1 s(y) p_{2n}(y) dy - (\alpha_2 - \alpha_i) \int_\eta^\rho s(y) p_{2n}(y) dy - (\alpha_2 - \alpha_1) \int_0^\eta s(y) p_{2n}(y) dy \right) \\
&= \alpha_2 s_{2n} - (4n+1) \left((\alpha_2 - \alpha_i) \int_\eta^\rho s(y) p_{2n}(y) dy + (\alpha_2 - \alpha_1) \int_0^\eta s(y) p_{2n}(y) dy \right).
\end{aligned}
\tag{32}
$$

5.1 Non-Smooth vector Field

The use of these functions in (19) leads to a nonsmooth vector field (Walsh 2017). We can separate the field into two sections, writing V^- for $\eta < \rho$ and V^+ for $\eta \geq \rho$. At $\eta = \rho$, $\bar{a}_{2n}(\rho) = \bar{b}_{2n}(\rho)$ and thus V^- and V^+ agree on the set

$$
\Sigma = \{(x,\eta) : x = (T_0, \ldots, T_{2N}), \eta = \rho\}
\tag{33}
$$

The set Σ is known as a switching boundary for the vector field V, defined as

$$
V(x,\eta) = \begin{cases} V^-(x,\eta), & (x,\eta) \in S^- \\ V^+(x,\eta), & (x,\eta) \in S^+ \end{cases}.
\tag{34}
$$

V is smooth on $\mathbb{R}^{N+2} \backslash \Sigma$, and continuous on $\mathbb{R}^{N+2}$ (Walsh 2017).

Walsh (2017) shows that while V is not C^1 at points in Σ, V is locally Lipschitz, which guarantees that the model ODE has unique solutions. As Fenichel's Theorem 3.1 applies only to smooth vector fields, we must restrict our analysis to two separate domains, $\eta < \rho$ and $\eta > \rho$.

5.2 Parameters and solutions

Due to more ice present, the diffusion of heat across latitudes (represented by the coefficient D) in the Neoproterozoic era would be less than our current climate. In Abbot, Voigt, and Koll (2011), they estimate $D = 0.25$. To justify this value, we estimated that for the Jormungand climate, we need a stable equilibrium at $\eta = 0.3$. This would place the ice line at a latitude of approximately $17.5°$.

Using $\eta = 0.3$ as the point of stable equilibrium, we can carry out similar calculations as in Section 4 to compute the diffusion coefficient D for varying N. For $N \geq 17$, $D = 0.3396$ to four decimal places. This is slightly higher than estimated in Abbot, Voigt, and Koll (2011), however still lower than the computed value for the two-step albedo model as expected.
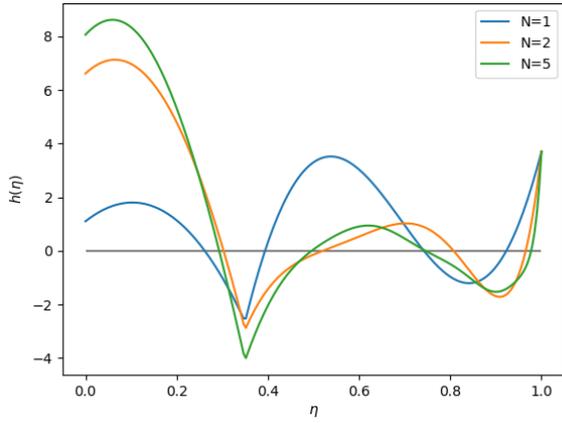
(a) Graph of $h(\eta)$, with α_J given by (28).
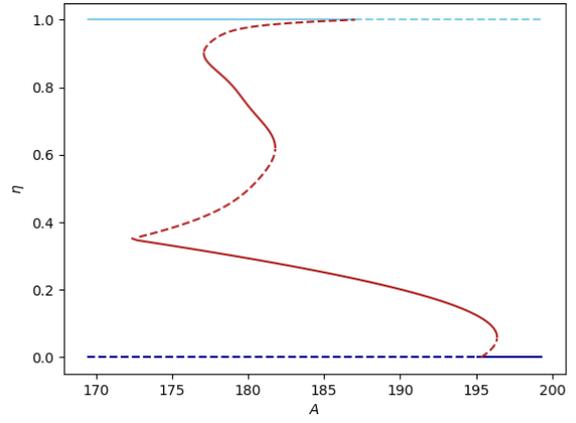
(b) The bifurcation diagram for A plotted for $N = 5$.

Figure 4: The Jormungand model depicts a climate where a large stable ice cap was present. The snowball state is no longer stable, making it much more plausible to reach our current climate. (a) Note large and small stable ice caps, and intermediate and very small unstable ice cap. Snowball state is unstable while the ice-free state is stable. (b) Dashed - unstable equilibria, solid - stable equilibria. Note the region of bi-stability approximately $A \in [177, 182]$. The large stable ice cap is present for a large range of A values.

As the climate also differed in the Neoproterozoic Era, the parameters were adjusted to account for this. The parameters were set as

$$Q = 321, A = 180, B = 1.9, \alpha_1 = 0.32, \alpha_i = 0.36, \alpha_2 = 0.8, T_c = -10, D = 0.3396. \tag{35}$$

In Figure 4, we have again plotted the function $h(\eta)$ as well as the bifurcation diagram for A. The dynamics figure shows both a large and small stable ice cap, as well as an intermediate unstable ice cap. The bifurcation diagram is plotted for $N = 5$, and shows that the large stable ice cap exists for a large range of A values, whereas the small stable ice cap only exists for a small range of A values. Note that our current value of $A = 202$ does not lie in this range, and thus this model does not accurately depict our current climate.

6   Continuous Albedo

In previous work (see Appendix), upon analysing the data on global albedo from Hummel and Reck (1979), we created the following continuous albedo function that better models the Earth's albedo:

$$\alpha_R(y, \eta) = \begin{cases} m(y, \eta) & y < \eta \\ n(y, \eta) & y > \eta \\ 0.47 & y = \eta \end{cases} \tag{36}$$

where $m(y, \eta) = 0.22y^2/\eta^2 + 0.25$ and $n(y, \eta) = 0.29(y - 1)/(1 - \eta) + 0.76$. That is, for the water albedo, a quadratic dependence on y is introduced, while the ice albedo follows a linear dependence. Again, computing the Legendre coefficients, we find

10
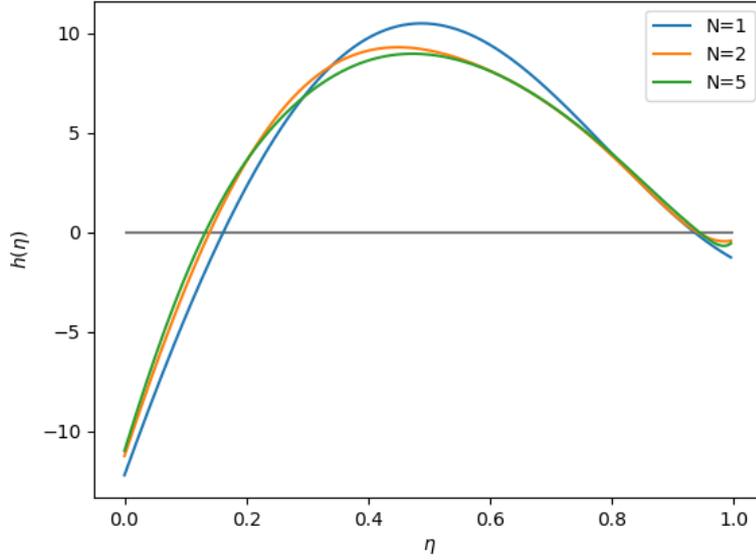
Figure 5: Graph of $h(\eta)$, using $\overline{\alpha}_{2n,R}$ given by (37). Parameters given by (27), with $D = 0.548$. Note one large unstable ice cap, one small stable ice cap, stable snowball earth state and unstable ice-free state.

$$\overline{\alpha}_{2n,R}(\eta) = (4n+1)\left(\int_0^{\eta} m(y,\eta)s(y)p_{2n}(y)dy + \int_{\eta}^1 n(y,\eta)s(y)p_{2n}(y)dy\right) \tag{37}$$

The system now reads

$$R\dot{T}_0 = Q\left(s_0 - \bar{\alpha}_{0,R}(\eta)\right) - A - BT_0 \tag{38a}$$

$$R\dot{T}_{2n} = Q\left(s_{2n} - \bar{\alpha}_{2n,R}(\eta)\right) - (B + 2n(2n+1)D)T_{2n}, n = 1, \ldots, N \tag{38b}$$

$$\dot{\eta} = \epsilon\left(\sum_{n=0}^N T_{2n}p_{2n}(\eta) - T_c\right) \tag{38c}$$

If $\epsilon = 0$, we once again have a globally attracting curve of rest points, and can thus apply Fenichel's Theorem 3.1 to approximate the system by the single ODE

$$\dot{\eta} = \epsilon\left(\sum_{n=0}^N f_{2n,R}(\eta)p_{2n}(\eta) - T_c\right) = \epsilon h(\eta) \tag{39}$$

Here, $f_{2n,R}$ is given by (23) however with $\overline{\alpha}_{2n,R}$ in replace of $\overline{\alpha}_{2n}$.

The dynamics can then be plotted as shown in Figure 5. The current climate was again fitted, and a diffusion coefficient of $D = 0.548$ ($N = 2$) was calculated.

When comparing Figure 5 with Figure 2, we note a similar qualitative shape to the curve. We also still see one small stable ice cap (at $\eta = 0.94$ by construction), and a large unstable ice cap at about $\eta = 0.15$. The snowball state is stable, however now the ice-free state is unstable, in contrast to the two-step albedo model. This indicates that the current small ice cap is less sensitive that predicted by the previous model.

7   Transition Model

Above, we have presented models that depict both the past and present climates. However, we would like a model that shows the transition from the past climate to our present climate. To do so, we create a transitional model, where the model used depends on the ice line. That is, we want a function such that for $\eta \leq 0.3$ (the estimated point of ice line stability for the Jormungand climate), the albedo is given only by α_J (28), and for $\eta \geq 0.94$ (the current point of ice line stability) the albedo is given by α_R (36). In between, the function is a straight line between the two points. We write

$$
\alpha_T = \begin{cases} \alpha_J, & \eta \leq 0.3 \\ \alpha_R + \frac{1}{0.64}(\alpha_R - \alpha_J)(\eta - 0.94), & 0.3 < \eta < 0.94 \\ \alpha_R, & \eta \geq 0.94 \end{cases} \tag{40}
$$

Then, it follows that, for $0.3 < \eta < 0.94$

$$
\overline{\alpha}_{2n,T}(\eta) = \overline{c}_{2n,T}(\eta) = \overline{\alpha}_{2n,R}(\eta) + \frac{1}{0.64}(\overline{\alpha}_{2n,R}(\eta) - \overline{\alpha}_{2n,J}(\eta))(\eta - 0.94)
$$

$$
= \overline{\alpha}_{2n,R}(\eta) + \frac{(\eta - 0.94)}{0.64}\left(\overline{\alpha}_{2n,R}(\eta) - \begin{cases} \overline{a}_{2n,J}(\eta), & \eta < \rho \\ \overline{b}_{2n,J}(\eta), & \eta \geq \rho \end{cases}\right). \tag{41}
$$

We also have that for $\eta \leq 0.3$, $\overline{\alpha}_{2n,T}(\eta) = \overline{\alpha}_{2n,J}(\eta)$ and for $\eta \geq 0.94$, $\overline{\alpha}_{2n,T}(\eta) = \overline{\alpha}_{2n,R}(\eta)$.

We can follow a similar analysis to that for the Jormungand albedo to show that the system can be well approximated by the single ODE, as above.

To determine the appropriate parameter values, we used a similar homotopy method in (40). This means that the parameters now depend of η as well. If X is an arbitrary parameter, and X_c, X_J are the current and Jormungand values of X respectively, then

$$
X(\eta) = \begin{cases} X_J, & \eta \leq 0.3 \\ X_c + \frac{X_c - X_J}{0.64}(\eta - 0.94), & 0.3 < \eta < 0.94 \\ X_c, & \eta \geq 0.94 \end{cases} \tag{42}
$$

This is used for parameters Q, A and D. $T_c = -10$ and $B = 1.9$ are held constant.

Figure 6 depicts the dyanmics of the model, through the graph of $h(\eta)$ and the bifurcation diagram for A. In Figure 6a, we see the large stable ice cap required for the Neoproterozoic climate, as well as the small stable ice cap depicting our current climate. We can also note that here both the snowball and ice-free states are unstable, eliminating the extremes. Figure 6b shows that the large stable ice cap is present for a large range of A values, while the small stable ice cap only exists for a small range of A values. This indicates that our current climate is very sensitive, and should we experience an increase in CO_2 such that A decreases beyond 200, the ice cap will begin to shrink before being pushed straight to the ice free state. Meanwhile, if we lose too much carbon dioxide from our atmosphere such that A increases beyond 203, then we will be pushed straight to the snowball state.

AMSI
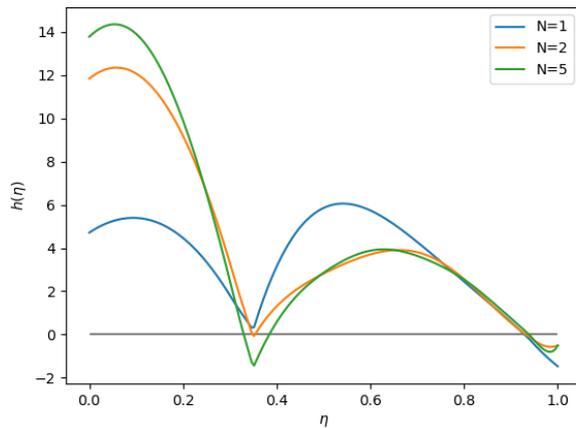
(a) Graph of $h(\eta)$, using $\overline{\alpha}_{2n,T}$ given by (41).
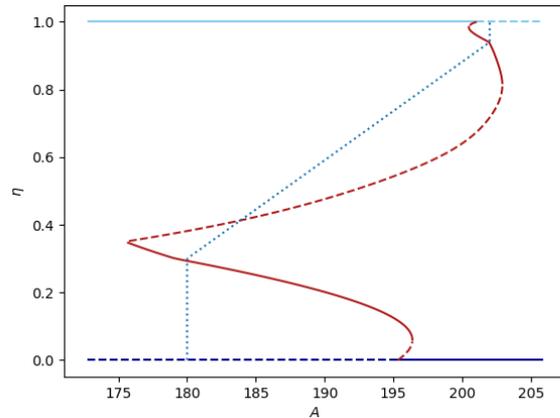
(b) Bifurcation diagram for A plotted for $N = 5$.

Figure 6: The transition model that depicts both the climate of the Neoproterozoic era and the present. Parameters given by (42). (a) Note the large and small stable ice caps, and intermediate unstable ice cap. Both the snowball and ice-free states are unstable. (b) Dashed - unstable equilibria, solid - stable equilibria. Dotted line - value of A through the homotopy given by (42). Note the small region of A values for which the small stable ice cap exists.

8   Conclusion

In this report, we have outlined the effect of a diffusion-based energy transport term on the results of the Budyko-Sellers Snowball Earth model. Combining this with the dynamic ice line model, we have produced results for various climates. Budyko's two-step albedo gave results that matched our current climate well, however failed to model the climate of the past and indicated stable snowball and ice-free states. An intermediate albedo value was introduced for the Jormungand model, which depicted a climate with a large stable ice cap, as theorised to have existed in Earth's past, however did not accurately model our current climate. Using a continuous albedo function developed in previous work, the results showed now an unstable ice-free state, which is potentially more realistic. Finally, the Jormungand and continuous albedos were combined in such a way to create the transition model, which depicted both the climate of the past, and the climate of the present.

Further research regarding this model could investigate non-fixed parameters such as A and Q. With the transition model, we have done this in a crude way, assuming that the parameters depend on the ice line. However, this is not realistic. Using variable parameters, a transition model could be developed in which the homotopy is driven by the parameters rather than the ice line, a much more realistic approach.

References

Abbot, Dorian S., Aiko Voigt, and Daniel Koll (2011). "The Jormungand global climate state and implications for Neoproterozoic glaciations". In: *Journal of Geophysical Research: Atmospheres* 116.D18. ISSN: 0148-0227.

Budyko, M. I (1969). "The effect of solar radiation variations on the climate of the Earth". In: *Tellus* 21.5, pp. 611–619. ISSN: 0040-2826.

Cloudy Earth (n.d.). https://earthobservatory.nasa.gov/images/85843/cloudy-earth.

Hoffman, Paul et al. (May 2020). *Snowball Earth.* `http://snowballearth.org`.

Hummel, John R. and Ruth A. Reck (1979). "A Global surface albedo model". In: *Journal of Applied Meteorology* 18.3, pp. 239–253.

McGehee, Richard and Clarence Lehman (2017). "A Paleoclimate Model of Ice-Albedo Feedback Forced by Variations in Earth's Orbit". In: *SIAM Journal on Applied Dynamical Systems* 11.2, pp. 684–707.

McGehee, Richard and Esther Widiasih (2014). "A Quadratic Approximation to Budyko's Ice-Albedo Feedback Model with Ice Line Dynamics". In: *SIAM Journal on Applied Dynamical Systems* 13.1, pp. 518–536. ISSN: 1536-0040.

North, Gerald R. (1975). "Analytical Solution to a Simple Climate Model with Diffusive Heat Transport". In: *Journal of the Atmospheric Sciences* 32.7, pp. 1301–1307. DOI: `10.1175/1520-0469(1975)032<1301: astasc>2.0.co;2`.

Sellers, William D. (1969). "A Global Climatic Model Based on the Energy Balance of the Earth-Atmosphere System". In: *Journal of Applied Meteorology (1962-1982)* 8.3, pp. 392–400. ISSN: 00218952, 2163534X. URL: `http://www.jstor.org/stable/26174552`.

"The Albedo of Clouds" (1911). In: *Popular Astronomy* 19, p. 591.

Walsh, James (2017). "Diffusive heat transport in Budyko's energy balance climate model with a dynamic ice line". In: *Discrete and Continuous Dynamical Systems Series B* 22.7, pp. 2687–2715.

Walsh, James and Richard Mcgehee (2013). "Modeling Climate Dynamically". In: *The College Mathematics Journal* 44.5, pp. 350–363. ISSN: 07468342.

Widiasih, Esther (2013). "Dynamics of the Budyko Energy Balance Model". In: *SIAM Journal on Applied Dynamical Systems* 12.4, pp. 2068–2092. ISSN: 1536-0040.

|	-180°	-170°	-160°	-150°	-140°	-130°	-120°	-110°	-100°	-90°	-80°	-70°	-60°	-50°	-40°	-30°	-20°	-10°	0°	10°	20°	30°	40°	50°	60°	70°	80°	90°	100°	110°	120°	130°	140°	150°	160°	170°	180°	Average
80°	66	66	66	66	66	66	66	66	66	66	66	66	71	71	70	68	66	66	66	66	66	66	66	66	66	66	66	66	66	66	66	66	66	66	66	66	66	66.37
70°	66	50	66	66	66	66	65	64	64	64	53	58	71	87	87	75	35	35	35	44	44	35	35	43	58	59	61	63	64	61	61	58	66	66	66	66	66	58.95
60°	33	38	54	54	54	42	45	52	58	45	44	45	34	75	34	29	35	35	35	37	41	41	37	41	42	44	46	46	30	38	46	46	50	52	51	37		43.42
50°	16	15	22	16	17	28	28	32	35	33	38	37	22	15	15	15	15	15	17	21	24	24	24	24	25	27	26	31	33	38	38	39	22	21	19	15		24.51
40°	9.1	9.1	9.1	9.1	9.1	15	25	26	26	22	23	15	10	9.1	9.1	9.1	9.1	14	13	13	14	14	17	22	28	25	24	26	25	24	24	17	12	9.2	9.1	9.1		16.12
30°	6	6	6	6	6	7.7	19	20	14	14	7.8	6	6	6	6	6	6.5	18	22	13	14	19	20	20	26	32	52	58	39	16	10	8	7.6	6	6	6		15.01
20°	4.9	4.9	5.2	4.9	4.9	4.9	6.8	17	6.6	6	6.7	4.8	4.8	4.8	4.8	4.8	18	31	23	26	26	18	26	27	9.4	16	14	11	18	12	6.8	4.9	4.9	4.9	4.9	4.9		11.19
10°	4.3	4.3	4.4	4.3	4.3	4.3	4.3	4.7	6.4	6	6.6	6.5	4.3	4.3	4.3	4.3	11	18	18	20	19	18	19	8	4.3	6.6	7.2	4.7	6	5.1	6	4.4	4.1	4.1	4.1	4.1		7.456
0°	4.1	4.1	4.1	4.1	4.1	4.1	4.1	4.1	4.1	4.3	11	11	7.4	4.1	4.1	4.1	4.4	6	7.3	9.2	9.5	16	15	4.5	4.1	4.1	4.8	4.1	6	5.7	5.6	4.5	4.1	4.1	4.1	4.1		5.847
-10°	4.1	4.1	4.1	4.1	4.1	4.1	4.1	4.1	5	5.6	8.4	7.8	11	11	8	4.1	4.1	4.1	4.1	9.3	9.5	16	5.5	4.1	4.1	4.1	4.1	4.1	5.2	5.8	5	4.9	5.8	4.9	4.2	4.1		5.733
-20°	4.4	4.3	4.3	4.3	4.3	4.3	4.3	4.3	4.3	4.3	10	14	15	17	6.4	4.3	4.3	4.3	4.3	14	17	15	8.4	5.6	4.3	4.3	4.3	4.3	4.3	4.3	7.2	14	11	4.7	4.4	4.4		7.003
-30°	4.9	4.9	4.9	4.9	4.9	4.9	4.9	4.9	4.9	4.9	6	19	17	11	5	4.9	4.9	4.9	4.9	13	20	10	7.8	5	4.9	4.9	4.9	4.9	4.9	7.5	25	28	21	13	4.9	5		8.642
-40°	6.5	6.1	6.1	6.1	6.1	6.1	6.1	6.1	6.1	6.1	8.5	17	12	6.2	6.1	6.1	6.1	6.1	6.1	6.7	10	6.4	6.1	6.1	6.1	6.1	6.1	6.1	6.1	7.1	12	9.9	14	10	6.1	7.3		7.433
-50°	9	9	9	9	9	9	9	9	9	9	12	15	9.1	9.1	9.1	9.1	9.1	9.1	9	9	9	9	9	9	9	9	9	9	9	9	9	9	9.7	9.2	9.2	11		9.35
-60°	15	15	15	15	15	15	15	15	15	15	16	11	19	19	23	26	26	26	26	25	24	21	18	16	15	15	15	15	15	15	15	15	15	15	15	15		17.53
-70°	36	36	35	35	35	35	35	35	35	36	38	53	42	46	46	46	45	43	43	45	45	43	49	52	50	49	55	56	56	55	55	52	52	44	40	37		44.08
-80°	53	53	51	61	69	72	73	73	78	76	81	85	56	53	53	60	78	85	85	85	85	85	85	85	85	85	85	85	85	85	85	85	85	85	81	56		75.2
-90°	85	85	85	85	85	85	85	85	85	85	85	85	85	85	85	85	85	85	85	85	85	85	85	85	85	85	85	85	85	85	85	85	85	85	85	85		85

Figure 7: The data given in Hummel and Reck (1979) shows the global albedo and latitudinal averages (right column), with a graded colour scale. Light: high albedo, dark: low albedo. The continents are visible, by the nature that land has a higher albedo than water. We can also see the lower albedo in regions of high ice cover, such as Greenland and the Himalayas. South America is not as visible due to the lower albedo caused by large rainforests.

A   Creating the Continuous Albedo

The following is taken from previous work by the author. Note that the model used considered a linear term for energy transport rather than the diffusion term used in the above report.

The albedo values used above are those used by Budyko (Budyko 1969), quoted to be correct "according to observational data available". However, Budyko took $\alpha(\eta, \eta) = 0.50$, not the average of the snow and water albedos used above, as suggested by Walsh and Mcgehee (2013).

Using the data given in Hummel and Reck (1979), an independent calculation for the albedo values was performed. Hummel and Reck (1979) gives the global albedo of our present Earth in a grid format with 10° latitude/longitude squares. Using a colour grading scheme, this data was utilised to produce Figure 7.

To align with the assumption on symmetry about the equator, the values for the northern and southern hemisphere were averaged. As the current ice line sits at about 72°, α_s was assumed to be an average of the albedo values from the poles until the $\pm 70°$ line, while α_w was taken to be an average of the albedo values from $-70°$ to 70°. This calculation gave the values

$$\alpha_w = 0.16 \quad \text{and} \quad \alpha_s = 0.71. \tag{43}$$

However, note that these values represent a cloud-free earth. The albedo of clouds varies with height and type of clouds, however the average is estimated to be 0.66 ("The Albedo of Clouds" 1911). If
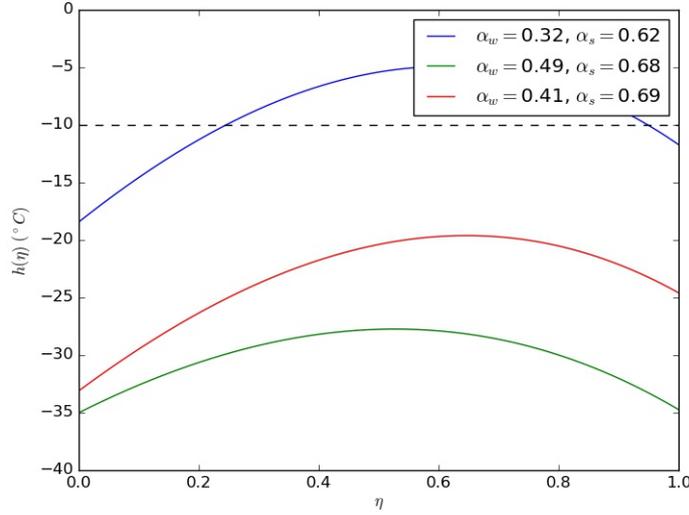
Figure 8: Temperature at the ice line with different values for α_w and α_s. Note that both cases of the calculated albedo values are well below the critical temperature, meaning that when considering a dynamic ice line, the only stable state would be the snowball state.

67% of Earth is covered with clouds on average (*Cloudy Earth* n.d.), then this gives

$$\alpha_w = 0.49 \quad \text{and} \quad \alpha_s = 0.68. \tag{44}$$

Furthermore, Budyko used the estimation that the Earth has 50% cloud cover, thus leading to the values

$$\alpha_w = 0.41 \quad \text{and} \quad \alpha_s = 0.69. \tag{45}$$

These values are not equal to those used by Budyko in Budyko (1969) (nor those used in Walsh and Mcgehee (2013)), and the impact of the difference is substantial, as shown by Figure 8. For both cases there is a lack of equilibrium values for which the temperature at the ice line is $-10°$C. These results demonstrate the sensitivity of the model to changes in albedo.

A more detailed look into the hemisphere averages reveals a somewhat parabolic shape up to the ice line, and linear beyond the ice line. This observation lead to the proposed albedo function

$$\alpha_R(y, \eta) = \begin{cases} 0.25y^2/\eta^2 + 0.36 & y < \eta \\ 0.15(y-1)/(1-\eta) + 0.76 & y > \eta \\ 0.62 & y = \eta \end{cases} \tag{46}$$

Here the end points are determined from the data in Hummel and Reck (1979), with 50% cloud coverage as suggested by Budyko. This function is plotted in Figure 9, along with the data values given for our current climate by Hummel and Reck (1979). Budyko's two-step function values are

16
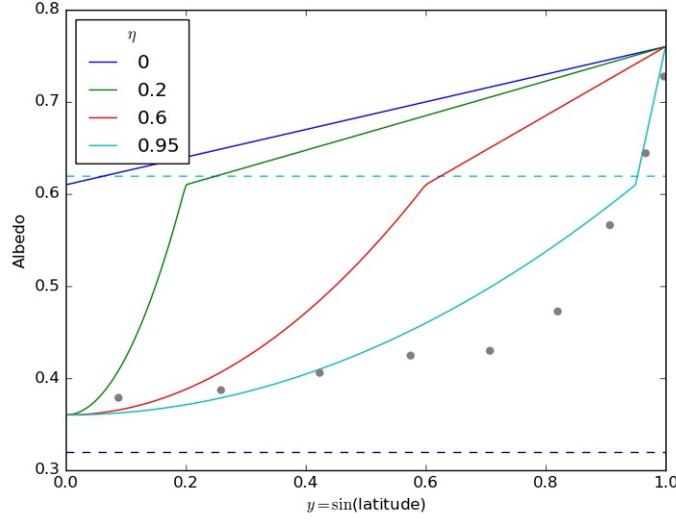
Figure 9: The parabolic/linear albedo function inspired by Hummel and Reck (1979). The solid lines give the function for various η values, while the dashed lines show how the function relates to Budyko's original values of $\alpha_w = 0.32$ and $\alpha_s = 0.62$. The data for our current climate ($\eta \approx 0.95$) from Hummel and Reck (1979) is plotted with grey points. Taking an average for $y > \eta$ and $y < \eta$ gives an approximation for the two-step function values. Here, that average is higher than Budyko's values.

also plotted for comparison. Note that the function average for each case is much higher than the values given by Budyko, similar to what was found above.

In order to replicate Budyko's results, the end and mid-points of the function are changed such that the function is now

$$
\alpha_{RB}(y, \eta) = \begin{cases} 0.22y^2/\eta^2 + 0.25 & y < \eta \\ 0.29(y-1)/(1-\eta) + 0.76 & y > \eta \\ 0.47 & y = \eta \end{cases} \tag{47}
$$

This gives Figure 10, which is comparable to Budyko's original function. This function can be used to plot similar graphs as those above, as shown in Figure 11.

The changes made between (46) and (47) have not been justified experimentally. However, values in Budyko (1969) are used to justify the adaptation. Alterations to other parameters such as A, Q or T_C would also correct the results obtained, however no experimental justification for doing so could be found.
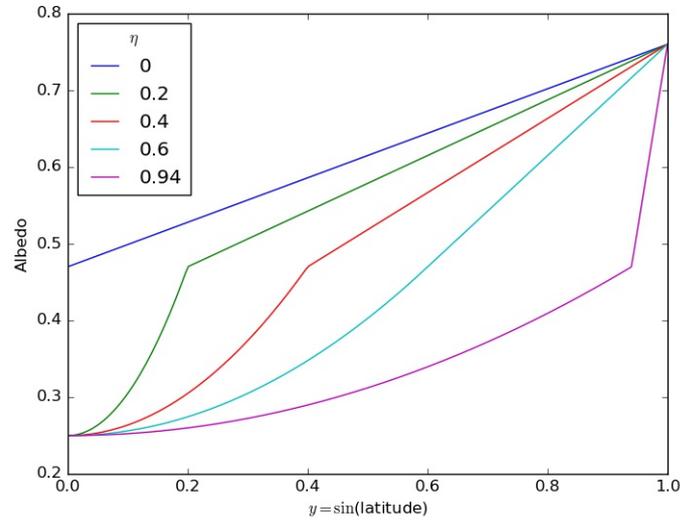
Figure 10: The parabolic/linear albedo function inspired by Hummel and Reck (1979) and adjusted such that the average values for both cases aligns better with Budyko's values. This adjustment has not been experimentally validated, however it is necessary for the function to be successfully applied to the Budyko model.
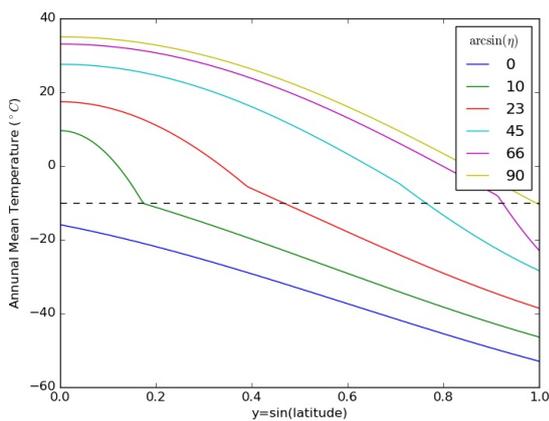
(a) Equilibrium profiles
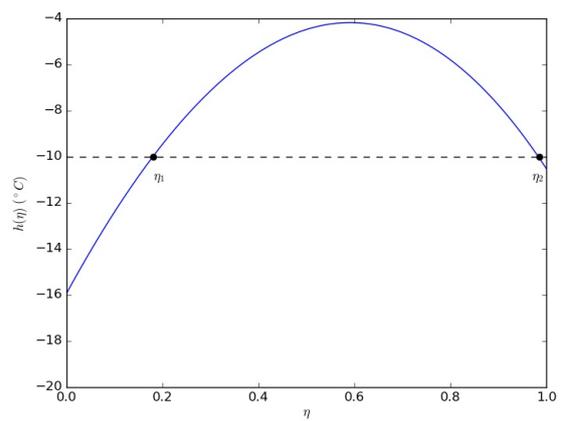
(b) Temperature at the ice line

Figure 11: Results produced when taking the albedo function to be given by (47).

AMSI